IEEE Access
Multidisciplinary | Rapid Review | Open Access Journal

Date of publication xxxx 00, 0000, date of current version xxxx 00, 0000.

Digital Object Identifier 10.1109/ACCESS.2017.Doi Number

Indoor Visible Light Positioning using Spring-Relaxation Technique in Real-World Setting

F. Alam[1], Senior Member, IEEE, N. Faulkner[1], M. Legg[1], S. Demidenko[1, 2], Fellow, IEEE

[1]Department of Mechanical & Electrical Engineering, School of Food and Advanced Technology, Massey University, Auckland 0632, New Zealand
[2]School of Science & Technology, Sunway University, Bandar Sunway, Selangor, Malaysia

Corresponding author: F. Alam (e-mail: f.alam@ massey.ac.nz).

This work was supported in part by Rexel Lighting and by the 2017-2018 Massey University Research Fund (MURF) under Grant "Implementation of an Asset Tracking & Monitoring System Leveraging Existing Wi-Fi & Lighting Infrastructure".

ABSTRACT GPS has limitations in indoor applications. Consequently, other indoor localization techniques and systems are an active area of research. Visible Light Positioning (VLP) is a promising option, especially given the growing popularity of LED-based lighting, and the expected adoption of the forthcoming Visible Light Communication (VLC). This paper reports a novel VLP technique. The developed technique uses received signal strength for the ranging. It is followed by the iterative estimation of a location using spring-relaxation. The performance of the proposed technique was experimentally evaluated in indoor settings and benchmarked against the lateration- and fingerprint-based localization approaches in multiple scenarios. The obtained results demonstrate that the proposed VLP approach offers an opportunity to outperform the existing techniques in terms of localization accuracy and precision.

INDEX TERMS Indoor localization, visible light positioning (VLP), indoor positioning system (IPS), received signal strength (RSS).

I. INTRODUCTION

Research and development in the area of *Indoor Localization* and *Indoor Positioning Systems* (IPS) have been highly intensive during the recent decade. Variety of technologies have been investigated for the indoor localization, e.g., *Light Detection and Ranging* (LIDAR) [1], *Image-Based* [2] , *Ultrasound-Based* [3]. One of the main shortcomings of such IPS solutions is the onus on the end-user to deploy the localization infrastructure. This is in a marked contrast to the *GPS-Based Outdoor Localization* [4] where an end-user can leverage the already existing infrastructure. It would be highly desirable if the IPS follows this GPS ethos, i.e., where the end- user would not be required to deploy any significant additional infrastructure resources.

Indoor localization leveraging the ubiquitous Wi-Fi [5] has achieved significant progress. However, the localization accuracy achieved while employing commercial off-the-shelf (COTS) equipment and cheap target tags is still limited to the order of meters [6]. Like most localization systems, Wi-Fi based IPS requires anchor nodes (*access points* (APs) for this case) at known locations. A preexisting Wi-Fi network that is deployed for data communication purposes is unlikely to have a large enough number of APs in any given region to meet the requirement of the IPS. The positioning based on other wireless technologies (e.g. *Bluetooth* [7], *ZigBee* [8], *RFID* [9] and *Ultra Wideband* (UWB) [10]) would normally require deployment of some bespoke network infrastructure. *Magnetic Fingerprinting-Based Localization* [11] is another option for the infrastructure-less positioning. However, it can be characterized as having rather poor accuracy. Besides, it is susceptible to ferromagnetic perturbations and requires significant efforts for the fingerprinting.

Visible Light Positioning (VLP) [12-14] has been put forward as a promising option, especially given the rapid uptake of LED-based energy-efficient lighting solutions and the promise of the upcoming *Visible Light Communication* (VLC) [15]. VLP is accepted to be far more accurate compared to the wireless based IPS and it has the potential to allow for localization while leveraging preexisting lighting infrastructure. Since a reasonably large number of luminaires are required for illumination purposes, it is conceivable that a lighting infrastructure consisting of LED luminaires could have the critical number of anchors required to provide localization. In this paper, a practical (i.e., real-world) VLP is reported that follows the GPS ethos of leveraging existing (lighting)

This article has been accepted for publication in a future issue of this journal, but has not been fully edited. Content may change prior to final publication. Citation information: DOI 10.1109/ACCESS.2019.2927922, IEEE Access

infrastructure while achieving accurate positioning of an object. Consumer grade LED luminaires are employed as transmitters and cheap photodiode (PD) -based receiver is utilized as a target tag. The developed system employs a novel (Spring-Relaxation) positioning technique.

II. RELATED WORK

A wide variety of signal characteristics can be utilized to localize a target. VLP systems based on Received Signal Strength (RSS) [16], Angle of Arrival (AOA) [17], Time of Arrival (TOA), Time Difference of Arrival (TDOA) [18], Phase Difference of Arrival (PDOA) [19], Differential Phase Difference of Arrival (DPDOA) [20] have been reported in the literature. Multiple signal characteristics like RSS and AOA have also been combined for localization purposes [21, 22]. AOA-based implementations generally require multiple photosensors or specialized optics. Time- and phase-based systems require highly synchronized hardware that increases the implementation cost. In contrast, RSS-based localization can be accomplished using a single photosensor-based target without requiring any synchronized hardware. This keeps the cost and complexity of implementation low and makes it ideal for realizing VLP systems while leveraging existing lighting infrastructure and cheap target tags.

RSS-based localization can be broadly categorized into *Proximity-* [23], *Model-* [24-26] and *Fingerprint-Based* [27, 28] techniques. While the proximity-based approach is easy to implement, its localization accuracy is quite poor since the coverage of the luminaire providing the strongest RSS is taken as the estimated position of the target. The model-based techniques use offline site survey to collect data for modelling the RSS-distance relationship. The calibrated model is used during the online or live stage for ranging. It is then followed by the position estimation through techniques like *lateration* [29]. The fingerprint-based techniques utilize the idea that a location can be uniquely identified by the RSS from the luminaires that are visible at that location. The fingerprint database is constructed during the offline stage through site surveying. The target is localized during the live stage operation through classifying the current RSS against the fingerprint database. Both model-based [25] and fingerprint-based [27] VLP systems have been shown to be quite accurate with median errors being in the sub decimeter range under controlled environment. However, fingerprint-based techniques may require extensive site surveying in order to achieve the required high localization accuracy.

With a few exceptions (e.g., work described in [30-32]), VLP systems reported in the literature employ exclusively LED based luminaires as transmitters or anchor nodes. Most works assume or utilize point sources. However, research work [33] looked into the impact of using linear or troffer sources on the optical channel model and employed them [34] for VLP systems. Work was also done to improve the localization accuracy by employing an optical antenna on the luminaires to optimize the luminous intensity distribution [35]. While, buzzword like Li-Fi has caught the imagination of the general public, VLC-enabled luminaires are not commercially available yet. Consequently, a vast majority of the VLP systems found in the literature are theoretical in nature while reporting their simulation-based results. The localization accuracy and precision reported in these studies may not be achievable for practical implementations under real-world conditions. Practical systems reported in the literature tend to employ specialized hardware [18] or bespoke luminaires [36]. Also they are often limited to small-scale testbeds [25],[37, 38] with experiments being conducted within a controlled environment [39].

Most VLP systems localize the target based on the information acquired from multiple luminaires (typically three or more). Each luminaire thus needs to have a unique identifier and the combined signal received from all the visible luminaires needs to be separated. Consequently, a VLP system needs a functional multiplexing/demultiplexing scheme. While upcoming VLC technologies are expected to provide sophisticated multiplexing schemes, researchers have had to develop their own paraphernalia in the interim. A variety of techniques like *On-Off Keying* (OOK) or *Square Wave Modulation* [40], *Orthogonal Frequency Division Multiple Access* (OFDMA) [41], discrete tone multiplexing based on *Intensity Modulation Direct Detection* (IM/DD) [28], *Optical Code Division Multiple Access* (OCDMA) [42] have been utilized. It should be pointed out that simulation based studies have shown that by employing smartphones [43], fusion of multiple sensors [22], and tags containing multiple photo-sensors [44], it might be possible to localize a target while employing just a single visible luminaire. Multiple photodiode-based localization systems have also been reported in [21], [45-47]. Visible light based localization was also fused with other techniques like wireless [48], magnetic fingerprinting [49], and inertial navigation sensors [50] to combat multipath degradation and loss of coverage due to occlusion. VLP system that does not require modification of the existing lighting fixtures has also been reported [51]. The system is based on computational imaging and sensor assisted photogrammetry technique therefore ideally requiring a smartphone as the VLP receiver, thus increasing its cost and somewhat restricting usability.

A wide variety of targets ranging from a PD [27] to a *solar cell* [40] have been utilized for VLP systems. Smartphones have been quite popular as they provide access to photosensors [24], camera [52], and inertial measurement unit [26]. However, smartphone as a VLP receiver has its limitations. It experiences occlusion in common use situations (e.g. when in the pocket). Besides, the relatively high cost makes it unsuitable for

This article has been accepted for publication in a future issue of this journal, but has not been fully edited. Content may change prior to final publication. Citation information: DOI 10.1109/ACCESS.2019.2927922, IEEE Access

implementations where large numbers of tags are required. There is a clear need for developing practical VLP systems so that positioning can potentially be offered as a secondary value-added service by the lighting infrastructure. Such VLP systems should employ COTS LED luminaires to leverage the existing lighting infrastructure. The localization algorithm could use RSS as the metric to avert employing complex bespoke systems. The tags need to be based on cheap PDs to facilitate the tracking of a large number of targets. The work presented in this paper brings all of these together in a novel way. The work is also exploring the possibility of employing the *Spring-Relaxation* (SR) algorithm for VLP. SR was successfully employed for localizing wireless sensor nodes [53-55]. Similar concepts termed potential fields and forced-based method were used for navigation of autonomous robots [56] and hybrid localization [48] respectively. A simulation study [57] shows that the location estimates of a fingerprint based VLP can be further improved by an SR algorithm based wireless positioning.

At the best of the authors' knowledge, this is the first reported work on VLP based on SR. It offers the following contributions:

a) First reported VLP system based on the Spring-Relaxation algorithm. The VLP system was developed and implemented while employing the RSS-distance model-based ranging followed by the localization using the SR technique;
b) Cost-effective VLP system leveraging existing lighting infrastructure. The luminaires are cost-effective COTS and the target is equipped with a cheap PD. The developed VLP system can be implemented with the existing LED-based lighting infrastructure with minimal modification. The proposed system can easily incorporate VLC enabled smart luminaires once they become commercially available. This would enable such a dual lighting/communication infrastructure to provide localization as a secondary service;
c) Benchmarked performance evaluation in multiple physical environments. The VLP system was implemented in two distinct physical environments. Unlike most reports in the literature, the proposed implementation includes two test-beds that are of a room scale with the following dimensions ($3.3\ m \times 2.1\ m \times 2.45\ m$) and ($7m \times 5\ m \times 2.45\ m$). The proposed SR algorithm was benchmarked against two existing algorithms while demonstrating its superior performance. The localization with median error of just *1.9 cm* was achieved.

The rest of the paper is organized as follows. Section III covers ranging and justifies the utilization of the Lambertian RSS-distance relationship for ranging based on experimental findings. The section also presents the proposed new SR algorithm for VLP. It demonstrates the algorithm within the context of the adopted experimental setup. Section IV describes the developed VLP system. It also outlines the two experimental setups, and presents the measurement data for both the setups. It is shown that the RSS-distance relationship for the two setups are dissimilar with the setup 2 exhibiting non-ideal signal attenuation characteristics. Section V displays the localization performance of the developed algorithm. The proposed SR algorithm is also benchmarked against two existing approaches. This section also reports the impact of various parameters on the SR algorithm. Section VI concludes the manuscript with some suggestions for the future work.

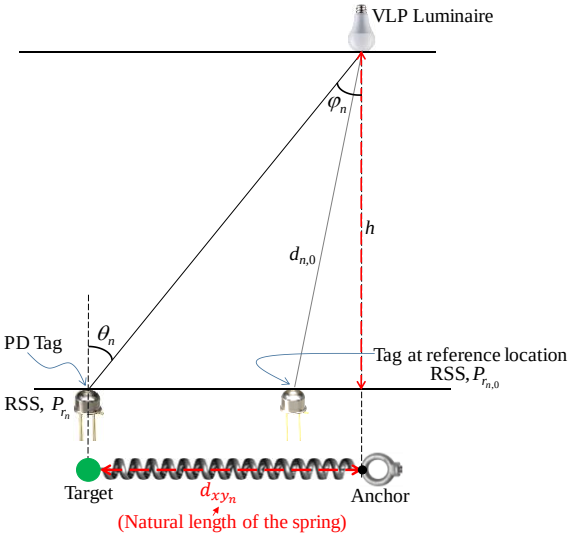

FIGURE 1. Parameters of the Lambertian model and relation with SR.

III. LOCALIZATION ALGORITHM

The proposed algorithm requires an offline stage where simple site surveying is conducted to calibrate the RSS-Distance model. During the live stage, ranging is performed while utilizing the calibrated model. The distance of the target from each visible luminaire is computed during the ranging. This is followed by the Spring-Relaxation based localization. The distances computed through the ranging are the "natural" lengths of the springs (explained in Section III B).

A. RANGING

Ranging is the technique of estimating the distance of the target from a set of fixed anchors (in this case - luminaires). For RSS based ranging, this involves modeling the signal received at the target as a function of a distance from the luminaire. Such modeling is performed for each luminaire based on the data collected during the offline calibration stage. During the live stage, the RSS reading is converted to a distance of the tag from each visible luminaire by

This article has been accepted for publication in a future issue of this journal, but has not been fully edited. Content may change prior to final publication. Citation information: DOI 10.1109/ACCESS.2019.2927922, IEEE Access

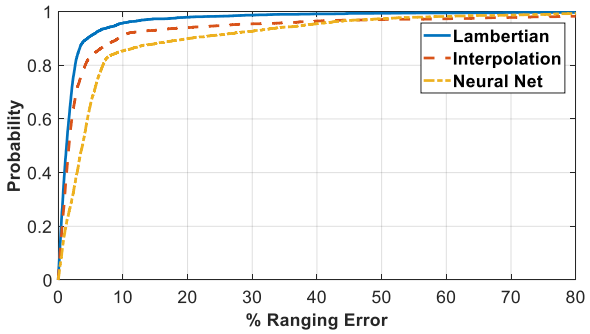

FIGURE 2. Ranging error of various methods for experimental setup 1. The median localization errors for Lambertian, interpolation and neural network approximation are 1.9, 4.1 and 6 cm respectively. Corresponding 95-percentile errors are 5.1, 12.3 and 12.1 cm.

inverting the respective calibrated attenuation model.

The received power P_{r_n} at a Line of Sight (LOS) location within the Field of View (FOV) of the PD that is d_n distance away from the *n*-th luminaire (see Fig.1) can be expressed by the generalized Lambertian model [58]

$$P_{r_n} = \frac{P_{t_n}}{d_n^2}\left(\frac{m_n+1}{2\pi}\right)\cos^{m_n}(\varphi_n)A\cos(\theta_n). \quad (1)$$

Here P_{t_n} is the transmitted power, m_n is the Lambertian order, φ_n is the irradiance angle, A is the physical area of the detector, and θ_n is the incidence angle. If the PD and the luminaries are parallel, it is relatively straightforward to simplify (1) as in [59] to

$$P_{r_n} = P_{r_{n,0}}\left(\frac{d_{n,0}}{d_n}\right)^{m_n+3}. \quad (2)$$

Here $P_{r_{n,0}}$ is the RSS at a reference location that is $d_{n,0}$ distance away (see Fig. 1) from the n th luminaire. During the offline stage, the Lambertian propagation model is calibrated using the method outlined in[59] by taking RSS measurement at a select small number of locations. Once m_n (the only unknown in (2)) is estimated through the calibration process, the ranging can be performed by rearranging (2) as

$$d_n = d_{n,0}\left(\frac{P_{r_{n,0}}}{P_{r_n}}\right)^{1/(m_n+3)}. \quad (3)$$

While the Lambertian model is quite popular for developing RSS-distance relationship and subsequent ranging, it is also possible to apply model-agnostic techniques (e.g., Neural Network-based function approximation or polynomial interpolation). Figure 2 compares the performance of the Lambertian-based technique with the model-agnostic ones for the experimental setup 1 (described in Section 4) by showing the *Cumulative Distribution Function* (CDF) of the ranging error. Quadratic polynomial was used for the interpolation. The Neural Network employed three hidden layers of the following sizes: 10, 8, 5, and *Bayesian Regularization* [60]. It can be observed that the ranging based on the Lambertian model outperforms the other two techniques. A similar trend was also observed for the second experimental setup. Consequently, the Lambertian model calibration based ranging was employed for the proposed localization algorithm.

B. 2D LOCALIZATION BY SPRING-RELAXATION

Once the distances between the target and each visible luminaire are computed by the ranging, the algorithm moves to iterative position estimation through the use of the Spring Relaxation technique. A set of fictitious springs are assumed to be connected between the target and corresponding spring anchors. The anchors are on the horizontal plane (parallel to the ceiling) containing the PD target and are located where the visible luminaires are. Each spring has a natural or relaxed length which is equal to the distance between the target and the anchor (see Fig.1). This natural length is found through the ranging (refer to (3) and (6)) that is based on the RSS at the target. At every iteration of the algorithm, the spring lengths, i.e., distances between the current estimated location of the target and the anchors, are computed. Each spring exerts a force on the target whenever it is compressed or stretched in accordance with Hooke's law. The magnitude of the force is proportional to the displacement of the spring from its natural length. The direction of the force is along the spring either pushing out or pulling the target towards the anchor depending on whether the spring is compressed or stretched. The spring-relaxation algorithm iteratively moves the target towards the direction of the net force, i.e., the vector sum of all the forces exerted by the springs. The localization algorithm stops when the net force exerted by the springs is zero or falls below a preassigned tolerance threshold.

Let us assume that the location of the n th luminaire or anchor is given in Cartesian and polar format respectively as

$$\overline{X_n} = x_n + jy_n = \rho_n e^{j\theta_n} = \rho_n \langle \theta_n . \quad (4)$$

Similarly, the estimated location of the target during the ith iteration is given as

$$\overline{X_T^i} = x_T^i + jy_T^i = \rho_T^i e^{j\theta_T^i} = \rho_T^i \langle \theta_T^i . \quad (5)$$

The natural length of the n th spring is d_{xy_n} and can be estimated as

$$d_{xy_n} = \sqrt{d_n^2 - h^2}. \quad (6)$$

Here the distance d_n is given by ranging as per (3) and h is the vertical distance between the PD and the luminaire. Please refer to Fig. 1 for an illustration of d_{xy_n}, d_n and h. The current length of the spring is given by

$$L_n = \left\| \overline{X_T^i} - \overline{X_n} \right\|. \quad (7)$$

This article has been accepted for publication in a future issue of this journal, but has not been fully edited. Content may change prior to final publication. Citation information: DOI 10.1109/ACCESS.2019.2927922, IEEE Access

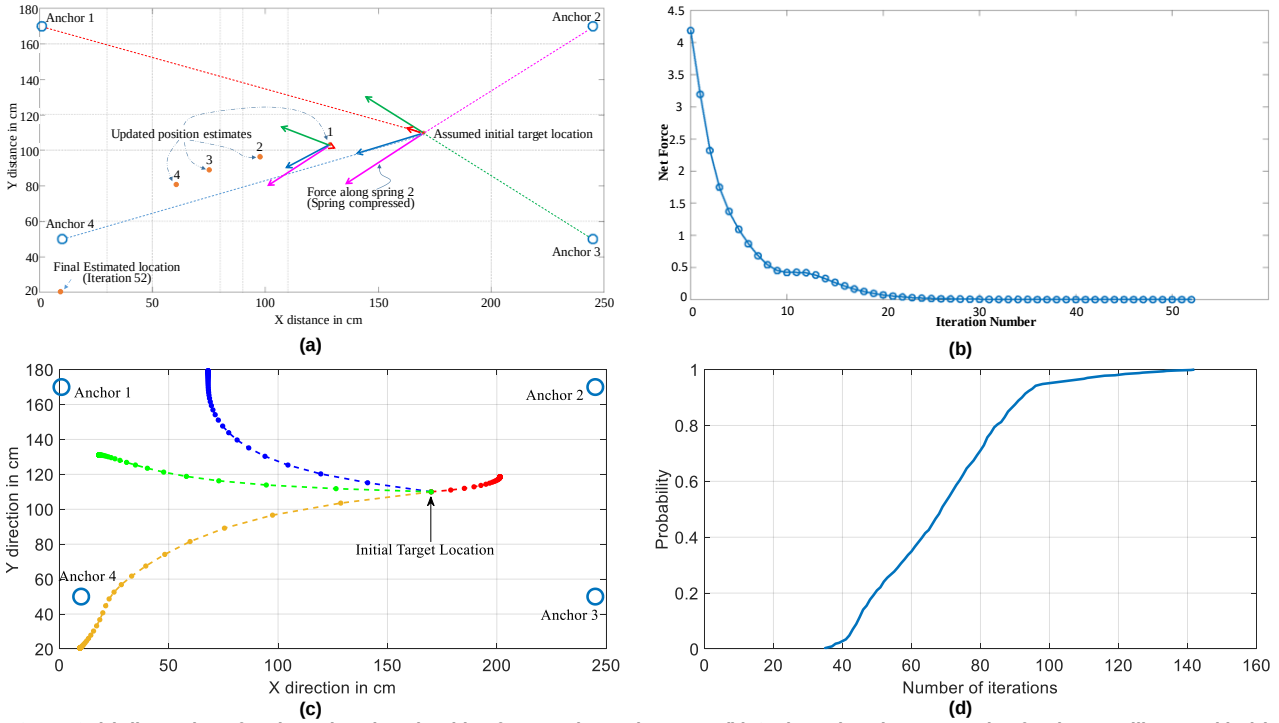

FIGURE 3. (a) Illustration of spring-relaxation algorithm for experimental setup 1; (b) Spring-relaxation converging for the case illustrated in (a); (c) Spring-relaxation for 4 arbitrary locations for experimental setup 1; (d) CDF of the number of iterations needed for SR algorithm to converge for 639 locations in experimental setup 1.The bottom most curve in (c) is the case illustrated in (a). All iterations start with an initial estimated location of 170+j110.

TABLE I
DETAILS OF THE ARTIFICIAL SPRINGS FOR THE CASE ILLUSTRATED IN FIG. 3(A). TOLERANCE, $\boldsymbol{\varepsilon}$ =10^{-4}. STEP SIZE, δ = 0.1

Natural length (cm)	Initial length (cm)	Initial Displacement (cm)	Initial Status	Final length (cm)	Final Displacement (cm)
148.6	179.3	30.7	Stretched	149.7	1.1
278.7	96.1	182.6	Compressed	279	0.3
237.6	96.1	141.5	Compressed	237.5	0.1
30.7	170.9	140.2	Stretched	29.4	1.3

Thus the displacement of the spring from the natural length is

$$\Delta_n = d_{xy_n} - L_n . \tag{8}$$

The magnitude of the force exerted by the spring is proportional to Δ_n. For this work, it is assumed that all the springs are identical. Hence it can be assumed that the magnitude of the force is equal to Δ_n. The force exerted on the target by the *n*th spring can now be computed as

$$\overline{F_n^i} = \Delta_n e^{j\phi_n} = \Delta_n \langle \phi_n . \tag{9}$$

Here ϕ_n is the angle between the vectors $\overline{X_T^i}$ and $\overline{X_n}$ i.e. $\phi_n = \text{angle}\left(\overline{X_T^i} - \overline{X_n}\right)$. The net force being exerted on the target is

$$\overline{F^i} = \sum_n \overline{F_n^i} . \tag{10}$$

At each iteration, the target's estimated location is moved a small distance in the direction of $\overline{F^i}$

$$\overline{X_T^{i+1}} = \overline{X_T^i} + \delta \overline{F^i} . \tag{11}$$

where δ is the step size. The algorithm keeps re-computing all the applied forces while also updating location estimate until a tolerance threshold is achieved so that

$$\left\| \overline{F^i} \right\| < \varepsilon \tag{12}$$

where ε is a predefined small constant.

Figure 3(a) illustrates application of the SR algorithm in the experimental setup 1. The actual location of the target is $\overline{X_T} = 10 + j20$. The algorithm starts with an assumed arbitrary initial target location at $\overline{X_T^0} = 170 + j110$ and terminates after 52 iterations with the final location estimated as $\overline{X_T^{52}} = 9.4 + j20.6$ and the localization error is 0.85 cm. Some of the relevant parameters for the

This article has been accepted for publication in a future issue of this journal, but has not been fully edited. Content may change prior to final publication. Citation information: DOI 10.1109/ACCESS.2019.2927922, IEEE Access

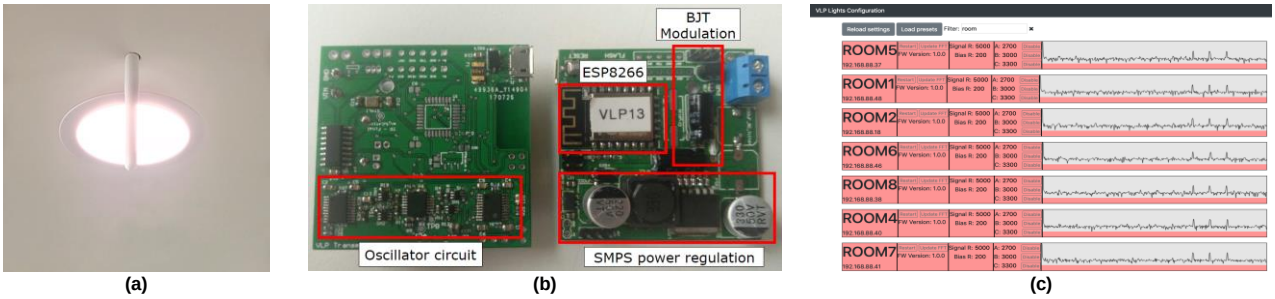

(a) (b) (c)

FIGURE 4. Details of the luminaires (transmitters) of the developed VLP system. (a) Installed luminaire with customised network connectivity. (b) Luminiare driver. Both sides of the PCB are shown. (c) Frontend GUI for Luminiare configuration

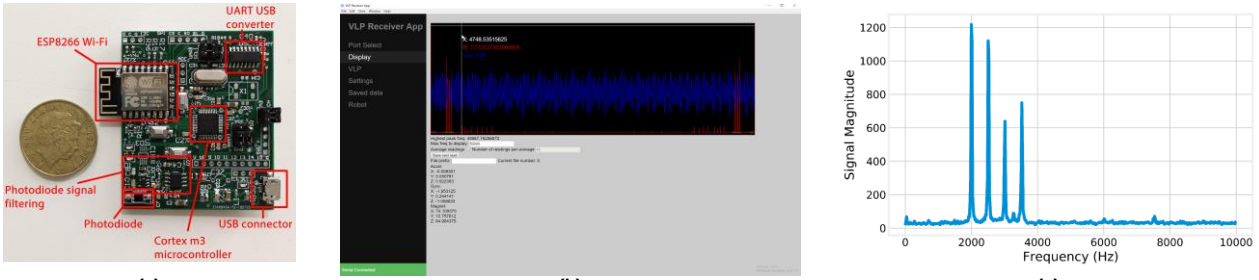

(a) (b) (c)

FIGURE 5. Details of the receiver tag of the developed VLP system. (a) Receiver tag. (b) Receiver app for data visualization. (c) RSS estimate using FFT

localization algorithm are shown in Table I. At the initial location, the springs 1 and 4 are stretched. They pull the target towards their respective anchors. Springs 2 and 3 are compressed. Consequently, they push the target away from the anchors. The force along spring 1 is much smaller compared to others as the displacement of the spring 1 is comparatively shorter. The net force moves the target to the interim location 1 ($\overline{X_T^1} = 128.7 + j103.5$). The forces are recalculated, and the location estimates are repeatedly updated until the 52-nd iteration, when the net force falls below the tolerance threshold, $\left\|\overline{F^{52}}\right\| = 8.9\times10^{-5} < \varepsilon$. The lengths of the springs are now very close to their respective natural lengths. Figure 3(b) shows the convergence of the SR algorithm after 52 iterations as the net force falls below the tolerance threshold. Figure 3(c) shows the iterative location estimation for four live locations with the same assumed initial location Figure 3(d) shows the CDF vs the number of iterations required for the algorithm to converge for all test locations in the experimental setup 1. The minimum, maximum, and median numbers of iterations required for the convergence are 35, 142 and 69 respectively for tolerance $\varepsilon = 10^{-4}$, and step size $\delta = 0.1$. However, it should be noted, the SR algorithm was initialized with the same initial location ($170+j110$) within the test space for the position estimation at every test location. Therefore, the statistics of the shown iteration numbers are exaggerated. For a real-world implementation, the initial location can be judiciously selected (e.g., a previously known location or location determined by coarse fingerprint based estimation) to reduce the number of iterations.

IV. Implementation of the VLP System and Experimental Setup

The developed VLP system includes consumer grade luminaires REX100DL WHWWDIM [61]. The discrete tone multiplexing based on IM/DD is employed. A custom designed circuit board (Fig. 4(b)) is inserted between each luminaire and its driver in order to transmit an unmodulated sinewave of a unique frequency between 2 KHz and 4 KHz. The amplitudes of the sinewaves are of orders of magnitude lower than the bias voltage. The flickering caused by the sinewaves is negligible, and it is also not perceptible to the human eye. The frequencies were selected so that there is no interference from the 100 Hz power line flicker caused by the existing lighting infrastructure. They were also chosen to be sufficiently high so to address possible concerns regarding potential health hazards of flickering at lower than 200 Hz frequencies[62]. The custom driver boards make use of an ESP8266 Wi-Fi equipped microcontroller [63] to control several Wien-bridge oscillators [64] to generate up to three simultaneous sinewave outputs. For the experiments conducted, each luminaire utilized only one sinusoid. However, the other two sinusoids could be used for a larger setup and data transmission using digital modulation techniques. Digital potentiometers on the oscillators are tuned by the custom-designed *proportional-integral* (PI) controllers to keep the generated sinewaves accurate within the ±5 Hz tolerance. Modified *switch mode power supply* (SMPS) and voltage regulator were used to power the ESP8266 microcontroller and other ICs. The additional

This article has been accepted for publication in a future issue of this journal, but has not been fully edited. Content may change prior to final publication. Citation information: DOI 10.1109/ACCESS.2019.2927922, IEEE Access

(a) (b)

FIGURE 6. The VLP system implemented at the two experiment locations. (a) Experimental setup 1. (b) Experimental setup 2

ATmega328p microcontroller [65] on the board is not used for the work presented here. It aims at providing an extra processing power for the future improvements and upgrades.

The *graphical user interface* (GUI) frontend (Fig. 4(c)) is developed to configure the parameters of each individual luminaire over Wi-Fi. This frontend is a web app running on a server that is accessible online. On power up, each luminaire contacts the server via the Wi-Fi module of the driver-board, and transmits its current local IP address. This allows for easy device discovery. It also enables adding new luminaires if required with very little extra effort. The web app (running in a web browser) can then communicate with any device on the same local network and send the requisite configuration data. A luminaire (that has been powered on and able to connect to the server) automatically appears on the front end. The receiver tag (Fig. 5(a)) consists of a photodiode, trans-impedance amplifier, and active high pass filter. The filter eliminates 100 Hz power-line flicker and the DC manifestation of the ambient light. The ambient light thus has no noticeable impact on the performance of the developed VLP as long as the light sensor is not saturated. A simple inverting amplifier stage then strengthens the filter output to a level suitable for *analog to digital conversion* (ADC). This signal is then fed to a microcontroller that carries out the ADC . The data can then be transmitted either via the onboard ESP8266 Wi-Fi module or, alternatively, via USB to a PC running a custom application to display and save the data. Whilst the ESP8266 has an inbuilt microcontroller, an external microcontroller is used to facilitate the high sampling rate of 50 KHz. This relieves the ESP8266 and helps it to maintain its primary function as the Wi-Fi communication module. The receiver also has an *Inertial Measurement Unit* (IMU) containing an accelerometer, gyroscope and magnetometer from which, the data can be sent alongside the photodiode data. The PC application (Fig. 5(b)) provides a live view of the received ADC value and the *Fast Fourier Transform* (FFT) for a defined number of samples. The app allows for recording snapshots of data to a *JavaScript Object Notation* (JSON) file [66] for a later use – either for replaying in the app or for processing in an external program such as MATLAB [67].

The demultiplexing is performed by using FFT that enables the measurement of the RSS of the received light at relevant frequencies corresponding to each visible luminaire. At the sampling rate of 50 KHz, it is possible to achieve a resolution of 12.2 Hz for the FFT based demultiplexing. Figure 5 (c) shows the RSS at the receiver tag at a location with four visible luminaires. The measured RSS is used for model calibration during the offline stage and for ranging during the live stage.

The VLP system was installed at two separate locations with ceiling height of *2.45 m* as shown in Fig. 6. The experimental setup 1 was in the (*5.7 m* × *4.8 m*) laboratory where the (*3.3 m* × *2.1 m*) rectangular space in the middle was used as the test field. The system consisted of four ceiling mounted luminaires whose locations along with the measurement locations are shown in Fig. 7. The RSS-distance model was calibrated based on the measurements performed at the 12 offline locations. The calibrations locations were chosen by following the guidelines presented in [59] while ensuring that each chosen offline location captures multiple regions of the Lambertian RSS-distance model for several luminaires. There were 639 additional locations within the test space, designated live locations, where RSS measurements were carried out to estimate the localization accuracy. There was no occlusion or obstruction within the test area and all four luminaires were within the FOV of the PD. This was a controlled experimental setup with doors and windows closed.

Experimental setup 2– the (*7.5m* × *8m*) open office foyer is shown in Fig. 6(b). It can be observed that there are some furniture items in the middle of the room and a photocopier along one wall. Left side of the room has a glass-wall with drawn light curtains. There is also a pillar in the middle of the room. The VLP system employs seven ceiling mounted luminaires. There were some restrictions as to where these

This article has been accepted for publication in a future issue of this journal, but has not been fully edited. Content may change prior to final publication. Citation information: DOI 10.1109/ACCESS.2019.2927922, IEEE Access

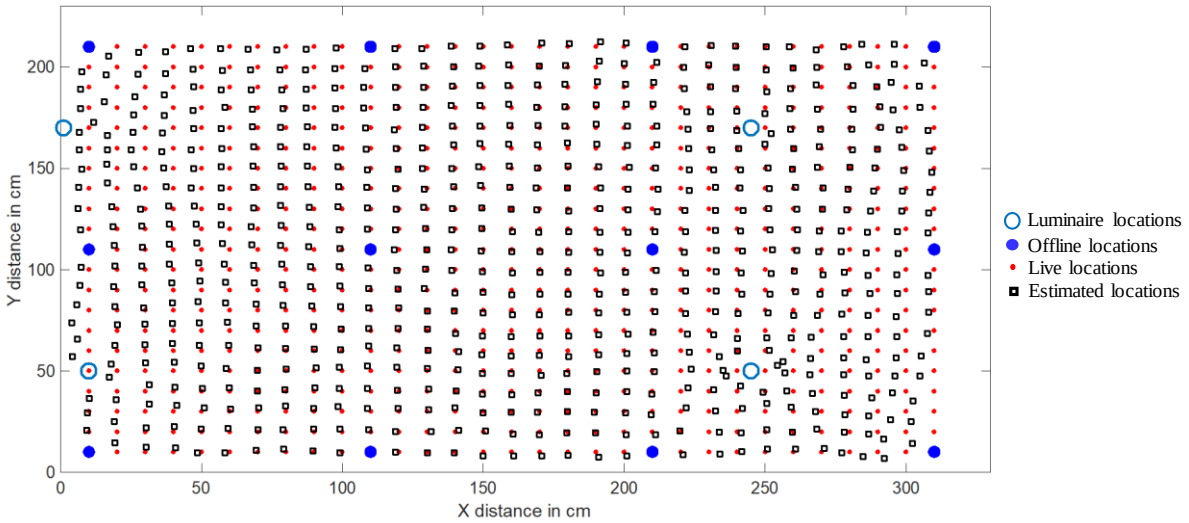

FIGURE 7. Layout of experimental setup 1. Offline locations show where the RSS measurement are taken for RSS-distance model calibration. Estimated locations are the estimates of the Spring-Relaxation algorithm for the live locations.

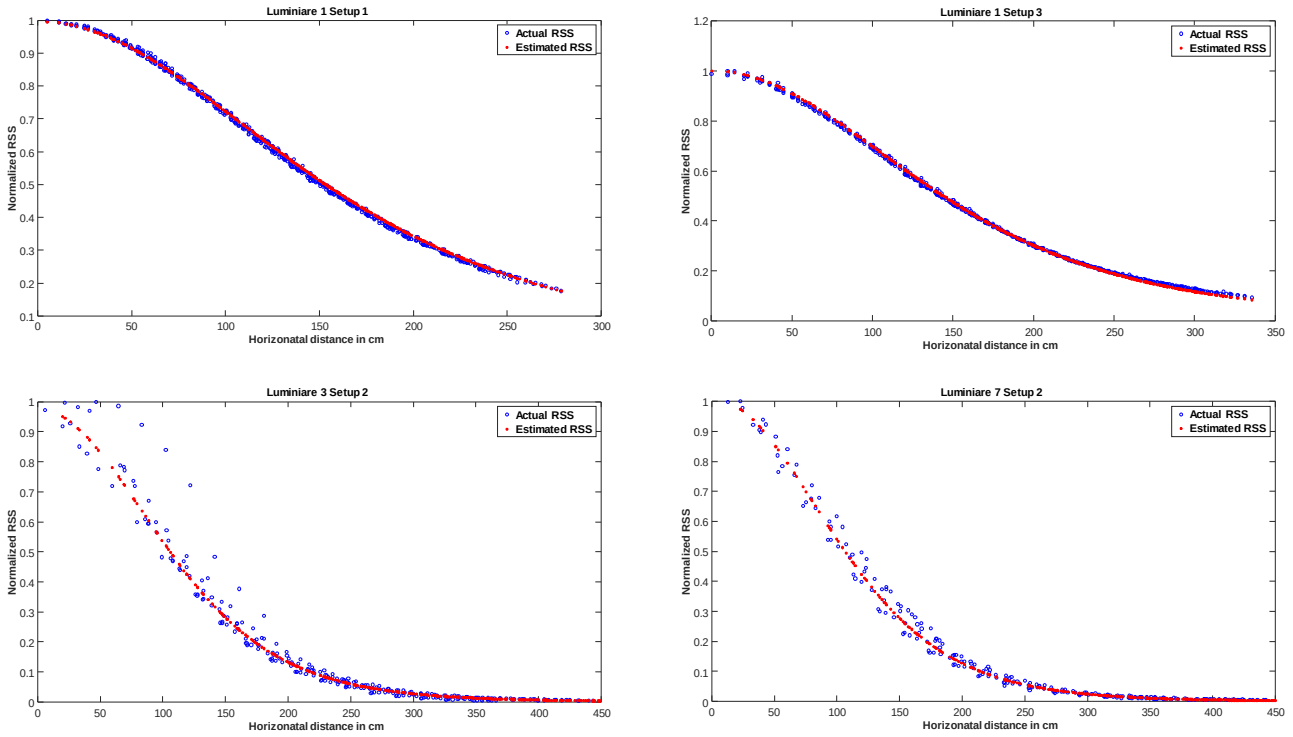

FIGURE 8. Actual and estimated RSS of different luminaires for both experimental setups. After calibration, equation 2 was used to estimate the RSS values

luminaires could be installed due to the presence of the ceiling florescent lights and air conditioner ducts. The RSS-distance model was calibrated based on 22 offline measurements. The localization accuracy was tested at 446 live locations.

Figure 8 shows the RSS-distance characteristics of various luminaires for both the experimental setups. It can be clearly observed that the RSS attenuation for the controlled experimental setup 1 quite closely follows the ideal Lambertian behavior. As a result, the RSS estimates are very accurate. Whereas the experimental setup 2 shows departure from the ideal characteristics. This is mainly due to multipath reflections and partial occlusions resulting from various objects within the test space and close proximity of the wall along some boundaries. Consequently, the localization error for the experimental setup 1 (reported in Section 5) is better by an order of magnitude. It should be noted that, for the localization experiments, it was possible to calibrate the RSS-distance model using 12 and 22 points respectively for all 4 and 7 luminaires respectively. The calibration process

This article has been accepted for publication in a future issue of this journal, but has not been fully edited. Content may change prior to final publication. Citation information: DOI 10.1109/ACCESS.2019.2927922, IEEE Access

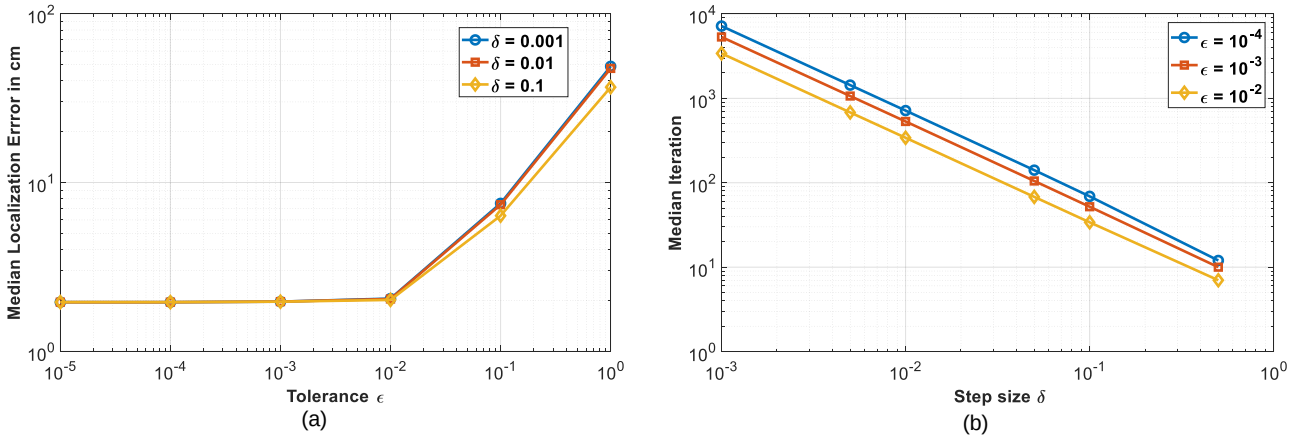

FIGURE 9. Impact of parameters ε and δ. Experimental setup 1. (a) Impact of tolerance, ε on localization accuracy. (b) Impact of step size δ on the number of iterations

scales efficiently and is relatively not labor intensive even for a large-scale implementation. While it is possible to achieve a slightly better approximation of the propagation model using a higher number of offline measurements, the impact on the localization error can be considered as being negligible.

V. LOCALIZATION RESULTS

The performance of the proposed algorithm was evaluated in the two environments described in Section 4. The localization error was evaluated as the median and the 95-percentile statistics as per the guidelines of EvAAL [68] and ISO/IEC 18305 [69]. Similarly, the precision is demonstrated as the empirical CDF of the localization error. The developed VLP system is capable of near real-time localization since the RSS data can be streamed over Wi-Fi in real time to the PC running the SR algorithm. The real-time capability of the system has been tested on multiple occasions. However, for the experiments conducted, the receiver was not truly mobile - it was moved manually from one location to another. This was done to accurately record the ground truth (the actual location of the receiver) that is needed in order to compute the error of the localization estimate.

A. EXPERIMENTAL SETUP 1

Figure 9(a) shows the impact of the tolerance parameter (ε) on the localization accuracy for various values of the step size (δ). As long as the value of ε is kept smaller than 10^{-2}, the step size has no noticeable impact on the localization accuracy. For larger values of ε ($>10^{-2}$), δ does show a small impact on the accuracy. However, this is inconsequential as ε values are to be kept lower than 10^{-2} in practical situations in order to keep the localization error small.

Figure 9(b) shows the impact of the step size (δ) on the number of iterations required by the SR algorithm. It can be observed that a bigger value of δ results in a smaller number of iterations. However, a large step size can result in instability, and the algorithm may fail to converge. For the adopted experimental scenario, δ needs to be kept smaller than 0.5 to ensure convergence.

Table II shows the localization accuracy of the proposed algorithm in terms of the median and 95-percentile errors. It is benchmarked against two existing algorithms. The first one is based on the ranging (similar to the SR algorithm as outlined in Section 3.1) and lateration. Localization is done by finding a least square solution of the lateration problem satisfying [58]

$$\overline{X_T} = \arg\min_{x_T, y_T} \sum_n \left[\sqrt{\left(x_T - x_n\right)^2 + \left(y_T - y_n\right)^2} - d_{xy_n} \right]^2. \quad (13)$$

The second algorithm used for benchmarking is based on fingerprint technique. *Weighted K-Nearest Neighbour* (WKNN) classifier [69] is used for target localization during the live stage. In order to have an objective comparison, a limited number of offline measurements is used to construct the fingerprint database by following the algorithm proposed in [27] and employing RSS regeneration. The Lambertian propagation model given by (2) is calibrated using the RSS at the offline calibration points shown in Fig. 5 just like it is done for the SR and lateration. The RSS-distance model is then used to regenerate fictitious RSS values to create a large fingerprint database corresponding to a *20cm* × *20cm* grid pattern covering the test space. The number of nearest neighbours (K) is equal to four for the WKNN classifier. It can be observed from Table II that for the experimental setup 1, the proposed SR algorithm outperforms the other two algorithms with significantly lower median and 95-percentile errors. Figure 10(a) shows the CDF of the localization error. Again, it can be observed that the proposed algorithm is more accurate when considered over the entire range. As it can be observed from Fig. 7, the localization estimate is more accurate in the middle of the testbed compared to the edges. This is due to the fact that the middle of the room is away from any reflectors (e.g., walls) and hence the RSS-distance characteristics follow the Lambertian model more truthfully in this region. This leads to a lower ranging error and,

This article has been accepted for publication in a future issue of this journal, but has not been fully edited. Content may change prior to final publication. Citation information: DOI 10.1109/ACCESS.2019.2927922, IEEE Access

TABLE II
LOCALIZATION ACCURACY OF THE PROPOSED SPRING-RELAXATION ALGORITHM FOR BOTH EXPERIMENTAL SETUPS; BENCHMARKED AGAINST LATERATION- AND WKNN REGENERATION BASED ALGORITHMS. $\boldsymbol{\varepsilon}$ =10^{-4} and δ= 0.01 for SR.

Localization accuracy, experimental setup 1						Localization accuracy, experimental setup 2					
Median Error (cm)			95-Percentile Error (cm)			Median Error (cm)			95-Percentile Error (cm)		
SR	Lateration	WKNN	SR	Lateration	WKNN	SR	Lateration	WKNN	SR	Lateration	WKNN
1.9	4	2.1	5.1	8.4	6.3	16.1	17.8	15.4	57.3	69.1	58.1

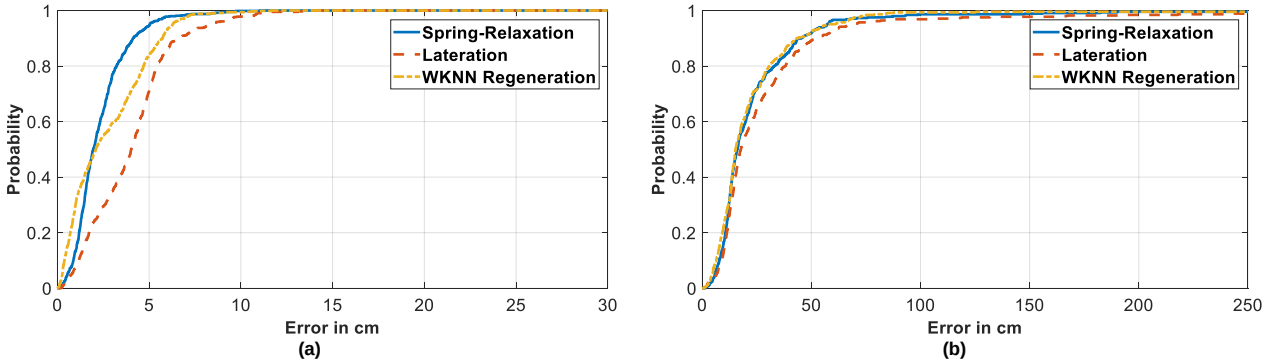

FIGURE 10. Comparison of localization precision as empirical CDF for experimental setup 1 and 2 respectively in (a) and (b). The Spring-Relaxation algorithm is benchmarked against the lateration- and WKNN regeneration based algorithms.

consequently, lower localization error. This trend was observed for all the three algorithms.

B. EXPERIMENTAL SETUP 2

Table II shows the benchmarked localization accuracy of the proposed algorithm. It can be observed that the localization accuracy of all the three algorithms degrade in this setup due to a non-ideal behavior of the RSS-distance relationship. The calibration is not as effective here. It is resulting in the larger ranging errors leading to the higher localization errors. However, the proposed algorithm still outperforms the lateration-based algorithm and is on par with the WKNN-based algorithm (producing the slightly larger median error against the smaller 95-percentile error).

Figure 11 shows the layout and other details of the experimental setup 2. The RSS-distance model for all the three algorithms was calibrated based on the measurements performed at the 22 locations (7 reference locations and 15 additional offline locations) marked in yellow. The localization accuracy was tested at 446 locations. It can be observed that for the majority of the test locations (381 out of 446), the localization error is less than 40cm for the SR algorithm. Some of the larger errors are around the furniture. This is probably due to the multipath reflections and partial occlusions in those locations. The two largest errors (>2m) are next to the lower edge of the test space. These are mainly due to the reflections from the curtains and partial occlusions from the nearby recycling bin. It should be noted that with continuous tracking, these large errors can be considered as an instant *teleportation* and can be mitigated through a geometric filter that rationalizes sudden large position change from one state to another. It can also be observed that there are some blind spots where at least three luminaires are not visible due to occlusion or the luminaries being outside of the PD's FOV. In locations where more than more than five luminaries are visible, the 4 luminaries corresponding to the highest RSS are selected as the anchors.

Figure 10(b) shows the CDF of the localization error: the proposed algorithm has better precision than the lateration-based algorithm, and it performs on par with the WKNN-based one.

1) ADVANTAGE OF SR OVER WKNN

The performance of the WKNN-based technique is heavily reliant on the parameter selection. Therefore, it has significant limitations in live localization applications. The localization accuracy of the WKNN algorithm varies significantly with the number of nearest neighbors, *K*, and the distance metric [27]. For both the experiments, *K*= 4 was used for the WKNN algorithm as that yielded the lowest localization error. Similarly, squared chord distance and squared chi-squared distance were chosen for experimental setups 1 and 2 respectively as they performed the best for the corresponding scenarios. These optimum parameters can only be selected based on a thorough fingerprinting of the test space and then computing the localization error for a variety of distances and *K* values at all test locations. This requires significant offline site survey often making it prohibitively expensive in terms of time and labor. The WKNN-based algorithm used here circumvents this cost by performing the few measurements for offline RSS-distance model calibration and subsequently regenerating the fingerprint database [27]. However, without the extensive offline site survey, the optimum value of *K* and the optimum distance metrics are not known a priori during the live stage in a real-world scenario. For the results presented involving the WKNN algorithm, the selection of *K* and the distance metric were

This article has been accepted for publication in a future issue of this journal, but has not been fully edited. Content may change prior to final publication. Citation information: DOI 10.1109/ACCESS.2019.2927922, IEEE Access

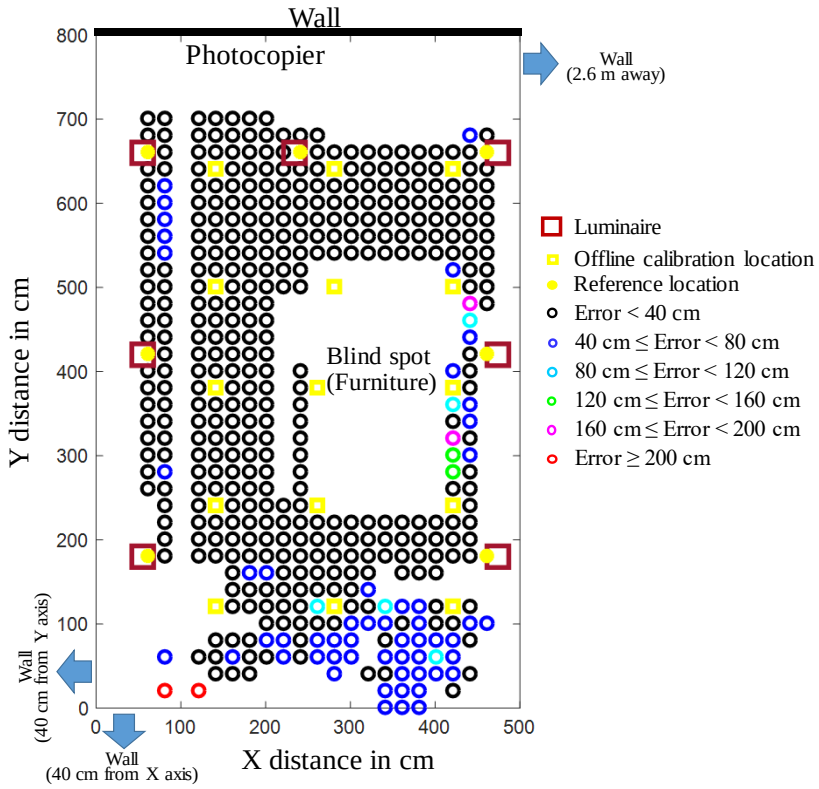

FIGURE 11. Layout and relevant details of the experimental setup 2. The localization errors are for the proposed SR algorithm.

made a posteriori i.e. after computing the localization error for a multitude of combinations involving distances and K values at all live locations. Whereas in a real-world scenario, the WKNN algorithm would have to use the standard Euclidean distance during the live stage as it is usually a safe choice having low performance variation with changing scenarios. This however results in higher localization errors for both experimental setups. For example in experimental setup 2, the median and 95-percentile localization error for Euclidean distance are 24.9 cm and 108.7 cm respectively, even with $K = 4$, making the performance significantly worse compared to the proposed SR algorithm. The localization accuracy further degrades if K is not chosen to be 4. In contrast, the localization accuracy of the proposed SR technique is relatively invariant to parameter selection as shown in Fig. 9(a). The handful of measurements performed for the RSS-distance model calibration is the only offline site survey that is required. Therefore, it can be inferred that the proposed SR technique is better suited to a practical environment compared to the WKNN-based algorithm.

VI. CONCLUSIONS

The novel real-world implementation of a VLP system is reported in this paper. Through the detailed experimental results, it is demonstrated that the Spring-Relaxation technique can be successfully utilized to localize a target carrying a low-cost PD-based tag by employing the RSS from the commercial off-the-shelf LED luminaires. The developed system provides median localization errors of 1.9 cm and 16.1 cm within two practical environments. The 95-percentile errors are 5.1 cm and 57.3 cm, respectively. The proposed approach significantly outperforms the lateration-based technique in both the experimental real-world environments. It also provides better localization accuracy than the fingerprint based technique in one implementation and is on par with it in the other environment.

In the presented work, it was assumed that all imaginary springs are identical. At the same time, the concept of a variable spring strength can be considered. It would assign different weights to each spring based on the confidence level associated with the RSS reading of the corresponding luminaire. The theoretical analysis of the convergence, stability and computational complexity of such an approach is planned for the future research.

The developed algorithm does not take into account previous location estimates when computing current locations. It can be expected that the application of continuous tracking could improve the accuracy of the developed system and make it more appropriate for mobile robotic applications. This is another area of interest for the planned future work.

It is also assumed in the reported research that the tag surface stays parallel to the ceiling. The future research will look into incorporating some types of tilt sensors to address other possible practical arrangements. The designed target

tag already has IMU onboard which can facilitate such research.

Finally, the future research can also employ improved attenuation model that accounts for multipath reflection and thereby improve localization performance through more accurate ranging.

ACKNOWLEDGMENT

The authors wish to thank Mr Baden Parr for his assistance in developing the hardware as well as Mr Ahmed Babader and Mr Tapiwanashe Wenge for their assistance in data collection.

REFERENCES

[1] M. Quigley, D. Stavens, A. Coates, and S. Thrun, "Sub-meter indoor localization in unmodified environments with inexpensive sensors," in *Intelligent Robots and Systems (IROS), 2010 IEEE/RSJ International Conference on*, Taipei, Taiwan, 2010, pp. 2039-2046: IEEE.

[2] J. Z. Liang, N. Corso, E. Turner, and A. Zakhor, "Image based localization in indoor environments," in *Computing for Geospatial Research and Application (COM. Geo), 2013 Fourth International Conference on*, 2013, pp. 70-75: IEEE.

[3] C. Medina, J. C. Segura, and A. De la Torre, "Ultrasound indoor positioning system based on a low-power wireless sensor network providing sub-centimeter accuracy," *Sensors*, vol. 13, no. 3, pp. 3501-3526, 2013.

[4] D. Wells *et al.*, "Guide to GPS positioning," in *Canadian GPS Assoc*, Fredericton,NB, Canada, 1987: Citeseer.

[5] S. He and S.-H. G. Chan, "Wi-Fi fingerprint-based indoor positioning: Recent advances and comparisons," *IEEE Communications Surveys & Tutorials*, vol. 18, no. 1, pp. 466-490, 2016.

[6] A. Yassin *et al.*, "Recent advances in indoor localization: A survey on theoretical approaches and applications," *IEEE Communications Surveys & Tutorials*, vol. 19, no. 2, pp. 1327-1346, 2016.

[7] Y. Zhuang, J. Yang, Y. Li, L. Qi, and N. El-Sheimy, "Smartphone-based indoor localization with bluetooth low energy beacons," *Sensors*, vol. 16, no. 5, p. 596, 2016.

[8] S.-H. Fang, C.-H. Wang, T.-Y. Huang, C.-H. Yang, and Y.-S. Chen, "An enhanced zigbee indoor positioning system with an ensemble approach," *IEEE Communications Letters*, vol. 16, no. 4, pp. 564-567, 2012.

[9] A. F. Errington, B. L. Daku, and A. F. Prugger, "Initial position estimation using RFID tags: A least-squares approach," *IEEE Transactions on Instrumentation and Measurement*, vol. 59, no. 11, pp. 2863-2869, 2010.

[10] A. Cazzorla, G. De Angelis, A. Moschitta, M. Dionigi, F. Alimenti, and P. Carbone, "A 5.6-GHz UWB position measurement system," *IEEE Transactions on Instrumentation and Measurement*, vol. 62, no. 3, pp. 675-683, 2013.

[11] B. Kim and S.-H. Kong, "A novel indoor positioning technique using magnetic fingerprint difference," *IEEE Transactions on Instrumentation and Measurement*, vol. 65, no. 9, pp. 2035-2045, 2016.

[12] J. Luo, L. Fan, and H. Li, "Indoor positioning systems based on visible light communication: state of the art," *IEEE Communications Surveys & Tutorials*, vol. 19, no. 4, pp. 2871-2893, 2017.

[13] M. Afzalan and F. Jazizadeh, "Indoor Positioning Based on Visible Light Communication: A Performance-based Survey of Real-world Prototypes," *ACM Computing Surveys (CSUR)*, vol. 52, no. 2, p. 35, 2019.

[14] Y. Zhuang *et al.*, "A survey of positioning systems using visible LED lights," *IEEE Communications Surveys & Tutorials*, vol. 20, no. 3, pp. 1963-1988, 2018.

[15] P. H. Pathak, X. Feng, P. Hu, and P. Mohapatra, "Visible light communication, networking, and sensing: A survey, potential and challenges," *IEEE communications surveys & tutorials*, vol. 17, no. 4, pp. 2047-2077, 2015.

[16] H. Lv, L. Feng, A. Yang, P. Guo, H. Huang, and S. Chen, "High accuracy VLC indoor positioning system with differential detection," *IEEE Photonics Journal*, vol. 9, no. 3, pp. 1-13, 2017.

[17] Y.-S. Kuo, P. Pannuto, K.-J. Hsiao, and P. Dutta, "Luxapose: Indoor positioning with mobile phones and visible light," in *Proceedings of the 20th annual international conference on Mobile computing and networking*, 2014, pp. 447-458: ACM.

[18] P. Du, S. Zhang, C. Chen, A. Alphones, and W.-D. Zhong, "Demonstration of a Low-complexity Indoor Visible Light Positioning System Using an Enhanced TDOA Scheme," *IEEE Photonics Journal*, 2018.

[19] A. Naz, H. M. Asif, T. Umer, and B.-S. Kim, "Pdoa based indoor positioning using visible light communication," *IEEE Access*, vol. 6, pp. 7557-7564, 2018.

[20] S. Zhang, W.-D. Zhong, P. Du, and C. Chen, "Experimental demonstration of indoor sub-decimeter accuracy VLP system using differential PDOA," *IEEE Photonics Technology Letters*, vol. 30, no. 19, pp. 1703-1706, 2018.

[21] S.-H. Yang, H.-S. Kim, Y.-H. Son, and S.-K. Han, "Three-dimensional visible light indoor localization using AOA and RSS with multiple optical receivers," *Journal of Lightwave Technology*, vol. 32, no. 14, pp. 2480-2485, 2014.

[22] Y. Hou, S. Xiao, M. Bi, Y. Xue, W. Pan, and W. Hu, "Single LED beacon-based 3-D indoor positioning using off-the-shelf devices," *IEEE Photonics Journal*, vol. 8, no. 6, pp. 1-11, 2016.

[23] Y. U. Lee and M. Kavehrad, "Two hybrid positioning system design techniques with lighting LEDs and ad-hoc wireless network," *IEEE Transactions on Consumer Electronics*, vol. 58, no. 4, 2012.

[24] P. Hu, L. Li, C. Peng, G. Shen, and F. Zhao, "Pharos: Enable physical analytics through visible light based indoor localization," in *Proceedings of the Twelfth ACM Workshop on Hot Topics in Networks*, 2013, p. 5: ACM.

[25] H.-S. Kim, D.-R. Kim, S.-H. Yang, Y.-H. Son, and S.-K. Han, "An indoor visible light communication positioning system using a RF carrier allocation technique," *Journal of Lightwave Technology*, vol. 31, no. 1, pp. 134-144, 2013.

[26] L. Li, P. Hu, C. Peng, G. Shen, and F. Zhao, "Epsilon: a visible light based positioning system," presented at the Proceedings of the 11th USENIX Conference on Networked Systems Design and Implementation, Seattle, WA, 2014.

[27] F. Alam, M. T. Chew, T. Wenge, and G. S. Gupta, "An Accurate Visible Light Positioning System Using Regenerated Fingerprint Database Based on Calibrated Propagation Model," *IEEE Transactions on Instrumentation and Measurement*, 2018.

[28] X. Guo, S. Shao, N. Ansari, and A. Khreishah, "Indoor localization using visible light via fusion of multiple classifiers," *IEEE Photonics Journal*, vol. 9, no. 6, pp. 1-16, 2017.

[29] J. Yang and Y. Chen, "Indoor localization using improved RSS-based lateration methods," in *GLOBECOM 2009-2009 IEEE Global Telecommunications Conference*, 2009, pp. 1-6: IEEE.

[30] C. Zhang and X. Zhang, "LiTell: robust indoor localization using unmodified light fixtures," in *Proceedings of the 22nd Annual International Conference on Mobile Computing and Networking*, New York City, New York, 2016, pp. 230-242: ACM.

[31] Z. Zhao, J. Wang, X. Zhao, C. Peng, Q. Guo, and B. Wu, "NaviLight: Indoor localization and navigation under arbitrary lights," in *INFOCOM 2017-IEEE Conference on Computer Communications, IEEE*, Atlanta, GA, USA, 2017, pp. 1-9: IEEE, 2017.

[32] S. Hamidi-Rad, K. Lyons, and N. Goela, "Infrastructure-less indoor localization using light fingerprints," in *Acoustics, Speech and Signal Processing (ICASSP), 2017 IEEE*

International Conference on, New Orleans, LA, USA, 2017, pp. 5995-5999: IEEE.

[33] J. Ding, Z. Xu, and L. Hanzo, "Accuracy of the point-source model of a multi-LED array in high-speed visible light communication channel characterization," *IEEE Photonics Journal*, vol. 7, no. 4, pp. 1-14, 2015.

[34] K. Qiu, F. Zhang, and M. Liu, "Visible light communication-based indoor environment modeling and metric-free path planning," in *Automation Science and Engineering (CASE), 2015 IEEE International Conference on*, Gothenburg, Sweden, 2015, pp. 200-205: IEEE.

[35] X. Huang, S. Guo, Y. Wu, and Y. Yang, "A fine-grained indoor fingerprinting localization based on magnetic field strength and channel state information," *Pervasive and Mobile Computing*, vol. 41, pp. 150-165, 2017.

[36] S. Liu and T. He, "SmartLight: Light-weight 3D Indoor Localization Using a Single LED Lamp," presented at the Proceedings of the 15th ACM Conference on Embedded Network Sensor Systems, Delft, Netherlands, 2017.

[37] J. Xu, C. Gong, and Z. Xu, "Experimental Indoor Visible Light Positioning Systems With Centimeter Accuracy Based on a Commercial Smartphone Camera," *IEEE Photonics Journal*, vol. 10, no. 6, pp. 1-17, 2018.

[38] X. Guo, F. Hu, R. Nkrow, and L. Li, "Indoor localization using visible light via two-layer fusion network," *IEEE Access*, 2019.

[39] H. Zheng, Z. Xu, C. Yu, and M. Gurusamy, "A 3-D high accuracy positioning system based on visible light communication with novel positioning algorithm," *Optics Communications*, vol. 396, pp. 160-168, 2017.

[40] C.-W. Hsu *et al.*, "Visible light positioning and lighting based on identity positioning and RF carrier allocation technique using a solar cell receiver," *IEEE Photonics Journal*, vol. 8, no. 4, pp. 1-7, 2016.

[41] B. Lin, X. Tang, Z. Ghassemlooy, C. Lin, and Y. Li, "Experimental demonstration of an indoor VLC positioning system based on OFDMA," *IEEE Photonics Journal*, vol. 9, no. 2, pp. 1-9, 2017.

[42] J. K. Park, T.-G. Woo, M. Kim, and J. T. Kim, "Hadamard matrix design for a low-cost indoor positioning system in visible light communication," *IEEE Photonics Journal*, vol. 9, no. 2, pp. 1-10, 2017.

[43] R. Zhang, W.-D. Zhong, Q. Kemao, and S. Zhang, "A single LED positioning system based on circle projection," *IEEE Photonics Journal*, vol. 9, no. 4, pp. 1-9, 2017.

[44] X. Yu, J. Wang, and H. Lu, "Single LED-Based Indoor Positioning System Using Multiple Photodetectors," *IEEE Photonics Journal*, vol. 10, no. 6, pp. 1-8, 2018.

[45] W. Xu, J. Wang, H. Shen, H. Zhang, and X. You, "Indoor positioning for multiphotodiode device using visible-light communications," *IEEE Photonics Journal*, vol. 8, no. 1, pp. 1-11, 2016.

[46] B. Xie *et al.*, "LIPS: A light intensity--based positioning system for indoor environments," *ACM Transactions on Sensor Networks (TOSN)*, vol. 12, no. 4, p. 28, 2016.

[47] L. Wei, H. Zhang, B. Yu, J. Song, and Y. Guan, "Cubic-receiver-based indoor optical wireless location system," *IEEE Photonics Journal*, vol. 8, no. 1, pp. 1-7, 2016.

[48] D. Konings, B. Parr, F. Alam, and E. M.-K. Lai, "Falcon: Fused Application of Light Based Positioning Coupled With Onboard Network Localization," *IEEE Access*, vol. 6, pp. 36155-36167, 2018.

[49] X. Wang, Z. Yu, and S. Mao, "DeepML: Deep LSTM for indoor localization with smartphone magnetic and light sensors," in *2018 IEEE International Conference on Communications (ICC)*, 2018, pp. 1-6: IEEE.

[50] Z. Li, A. Yang, H. Lv, L. Feng, and W. Song, "Fusion of visible light indoor positioning and inertial navigation based on particle filter," *IEEE Photonics Journal*, vol. 9, no. 5, pp. 1-13, 2017.

[51] S. Zhu and X. Zhang, "Enabling high-precision visible light localization in today's buildings," in *Proceedings of the 15th Annual International Conference on Mobile Systems, Applications, and Services*, 2017, pp. 96-108: ACM.

[52] J.-K. Lain, L.-C. Chen, and S.-C. Lin, "Indoor Localization UsingK-Pairwise Light Emitting Diode Image-Sensor-Based Visible Light Positioning," *IEEE Photonics Journal*, vol. 10, no. 6, pp. 1-9, 2018.

[53] Q. Zhang, C. H. Foh, B.-C. Seet, and A. C. M. Fong, "Location estimation in wireless sensor networks using spring-relaxation technique," *Sensors*, vol. 10, no. 5, pp. 5171-5192, 2010.

[54] Q. Zhang, C. H. Foh, B.-C. Seet, and A. Fong, "Variable elasticity spring-relaxation: improving the accuracy of localization for WSNs with unknown path loss exponent," *Personal and Ubiquitous Computing*, vol. 16, no. 7, pp. 929-941, 2012.

[55] H. Li, Y. Hu, and M. Zhu, "Sliding-mode and spring-relaxation-like technique for location estimation in wireless sensor networks," *International Journal of Distributed Sensor Networks*, vol. 8, no. 8, p. 283524, 2012.

[56] B. Li, H. Du, and W. Li, "A Potential field approach-based trajectory control for autonomous electric vehicles with in-wheel motors," *IEEE Transactions on Intelligent Transportation Systems*, vol. 18, no. 8, pp. 2044-2055, 2017.

[57] Z. Luo, W. Zhang, and G. Zhou, "Improved spring model-based collaborative indoor visible light positioning," *Optical Review*, vol. 23, no. 3, pp. 479-486, 2016.

[58] W. Gu, M. Aminikashani, P. Deng, and M. Kavehrad, "Impact of multipath reflections on the performance of indoor visible light positioning systems," *Journal of Lightwave Technology*, vol. 34, no. 10, pp. 2578-2587, 2016.

[59] F. Alam, B. Parr, and S. Mander, "Visible Light Positioning Based on Calibrated Propagation Model," *IEEE Sensors Letters*, vol. 3, no. 2, pp. 1-4, 2018.

[60] F. Burden and D. Winkler, "Bayesian regularization of neural networks," in *Artificial neural networks*: Springer, 2008, pp. 23-42.

[61] (March 05, 2019). *RX 13 LED Downlight*. Available: https://www.rexellighting.co.nz/products/rx-13-led-downlight

[62] A. Wilkins, J. Veitch, and B. Lehman, "LED lighting flicker and potential health concerns: IEEE standard PAR1789 update," in *Energy Conversion Congress and Exposition (ECCE), 2010 IEEE*, 2010, pp. 171-178: IEEE.

[63] (March 05,2019). *ESP8266 Technical Reference*. Available: https://www.espressif.com/sites/default/files/documentation/esp8266-technical_reference_en.pdf

[64] L. Arguimbau, "An oscillator having a linear operating characteristic," *Proceedings of the Institute of Radio Engineers*, vol. 21, no. 1, pp. 14-28, 1933.

[65] (March 05, 2019). *ATmega48A/PA/88A/PA/168A/PA/328/P Data Sheet*. Available: http://ww1.microchip.com/downloads/en/DeviceDoc/ATmega48A-PA-88A-PA-168A-PA-328-P-DS-DS40002061A.pdf

[66] D. Crockford, "The application/json media type for javascript object notation (json)," 2070-1721, 2006.

[67] H. Moore, *MATLAB for Engineers*. Pearson, 2017.

[68] F. Potortì *et al.*, "Comparing the performance of indoor localization systems through the EvAAL framework," *Sensors*, vol. 17, no. 10, p. 2327, 2017.

[69] M. B. Christopher, *PATTERN RECOGNITION AND MACHINE LEARNING*. Springer-Verlag New York, 2016.